Submitted to
32nd International Conference on High Energy Physics, ICHEP04, August 16, 2004, Beijing
Abstract: **5-0165**
Parallel Session **5**
www-h1.desy.de/h1/www/publications/conf/conf_list.html

Measurement of Beauty Production in Deep Inelastic Scattering at HERA

H1 Collaboration

Abstract

Differential measurements of beauty electroproduction cross sections in ep collisions performed with the H1 detector at HERA are presented. The data were collected at an ep centre-of-mass energy of 319 GeV in the years 1999-2000 and correspond to an integrated luminosity of 50 pb^{-1}. Events are selected by requiring at least one high-transverse momentum jet in the Breit frame with $p^*_{t,jet} > 6$ GeV, jet pseudorapidity $|\eta^{jet}| < 2.5$ and a muon associated to the jet with $-0.75 < \eta^{\mu} < 1.15$ and $p_t^{\mu} > 2.5$ GeV. Both the lifetime signature and the large mass of b-flavoured hadrons are exploited to determine the fraction of events in the sample containing beauty. Differential jet-muon cross sections are measured in the region of photon virtuality $2 < Q^2 < 100$ GeV^2 and inelasticity $0.1 < y < 0.7$. The results are compared with different Monte Carlo models and with calculations in NLO perturbative QCD.

1 Introduction

This paper presents a measurement of open beauty production in ep collisions in deep inelastic scattering where the photon virtuality $Q^2 > 2\,\text{GeV}^2$. b-quark production is an interesting testing ground for perturbative QCD (pQCD) since the large mass of the b-quark provides a hard scale. Towards larger Q^2 and/or p_t the interplay between the different hard scales can be investigated.

Early measurements, both in photoproduction [1–3] and in deep inelastic scattering, indicated that the beauty production cross section lies significantly above the next-to-leading order QCD expectations. Similar observations have been made in hadron-hadron collisions [4], and also in two-photon interactions [5]. While for some of the above measurements large extrapolations beyond the measurable kinematic range were performed using Monte Carlo simulations, the more recent measurements reported visible cross sections, $e^+p \rightarrow e^+b\bar{b}X \rightarrow e^+ + jets + \mu^\pm + X$, [6, 7] within the accessible detector acceptance. To compare with next-to-leading order perturbation theory the theoretical calculations were interfaced with parametrized b-quark fragmentation and muon decay spectra in order to impose the same kinematic constraints as for the measurements. Comparisons between the measured and calculated visible cross sections then showed reasonable agreement between data and theory.

In this paper a new measurement of beauty production in ep scattering is presented. Events with at least one jet and a muon in the final state are used to measure the beauty production cross section $e^+p \rightarrow e^+b\bar{b}X \rightarrow e^+ + jet + \mu^\pm + X$. The cross section is measured differentially as a function of the photon virtuality Q^2, the Bjorken scaling variable $x = Q^2/sy$ and the transverse momentum of the b-quark jet in the Breit frame, p_t^*, jet. Here s is the ep center of mass energy and y the fractional energy of the exchanged photon in the proton rest-frame. The differential cross section is also measured as a function of the transverse momentum of the b-quark jet in the Breit frame.

For the measurement both the lifetime signature and the large mass of b-flavoured hadrons are used to determine the fraction of beauty quark events in the sample. The fraction of b-quark events in the final sample is determined by a fit to the two-dimensional distribution of the p_T^{rel} and δ observables in the data with adjustable fractions of beauty, charm and light-quark components, the shapes of which are taken from Monte Carlo (MC) simulations. The experimental procedure follows closely the one described in detail in [7]. This paper is organised as follows: The event selection is described in section 2. The Monte Carlo simulations and data sets used to model the signal and background components of the data are described in section 3. In section 5 the signal determination observables and procedure are outlined. In section 4 the calculations in perturbative QCD performed at next-to-leading order are explained. The measured cross sections are presented in section 6 and compared with predictions from Monte Carlo simulations and pQCD.

2 Event Selection

The H1 Experiment is described in detail in [8–10]. The data for this analysis were recorded in 1999 and 2000 and correspond to an integrated luminosity of $50\,\text{pb}^{-1}$. The events were

triggered by requiring the coincidence of signals from the scattered electron in the calorimeter, and tracks in the central drift chambers (CJC) and the multi-wire proportional chambers. Events are selected by requiring that there be at least one high energetic ($E > 8$ GeV) electromagnetic cluster in the backward calorimeter. The accepted range of negative four-momentum transfer squared is restricted to $2 < Q^2 < 100$ GeV^2. An inelasticity cut $0.1 < y < 0.7$ is applied, where y is calculated using the Sigma method [11], which reduces sensitivity of the kinematic reconstruction to QED-radiation off the incoming beam electron. Jets are reconstructed in the Breit frame using the inclusive k_t algorithm [12] with radius $R = 1$ in the η-ϕ plane. The E_T-recombination scheme is applied giving massless jets. The selection requires at least one jet with transverse energy in the Breit frame of $p^*_{t,jet} > 6$ GeV, which contains a muon candidate. Muons are identified as tracks in the barrel part of the instrumented iron return yoke, linked to the drift chamber track with a link-probability larger than 5%, and are required to have a transverse momentum of $p^\mu_t > 2.5$ GeV. The iron barrel acceptance corresponds to polar angles $35^\circ < \theta(\mu) < 130^\circ$. The measurement of the impact parameter is facilitated by the high precision tracking made possible with the H1 central silicon tracker (CST). At least two CST-r-ϕ-hits must be associated with the muon candidate track, measured in the central drift chambers. The combined CJC-CST r-ϕ-track fit probability must exceed 10%. The final event sample consists of 780 events.

3 Monte Carlo Simulations and Control Data Samples

Monte Carlo event samples for the processes $ep \to eb\bar{b}X$, $ep \to ec\bar{c}X$ and light quark production are generated using the RAPGAP program [13] which is based on leading order QCD and parton showers. In RAPGAP the charm and beauty quarks are produced via boson-gluon fusion (massive approach). RAPGAP implements QED radiation effects. The light quark sample is used to simulate the background from fake muons, i.e. hadrons misidentified as muons, and decays of light mesons into muons. The CTEQ5L [14] parton densities are used for the proton. The programs PYTHIA [15] and CASCADE [16] are used for cross checks. PYTHIA simulates direct and resolved photon processes and also includes excitation processes, in which one heavy quark (c or b) originates from the resolved photon or the proton. PYTHIA is run in an inclusive mode and generates all the above processes using massless matrix elements. CASCADE is a Monte Carlo generator which implements the CCFM parton evolution equation [17]. The Monte Carlo simulation programs have been checked to accurately describe the detector resolutions, efficiencies and acceptances.

4 Predictions Based on QCD NLO Calculations

The program HVQDIS for NLO calculations by B.W.Harris and J.Smith [18] was modified to facilitate the comparison of the calculation with the visible cross sections in the experimentally accessible kinematic range. The outgoing partons (b-quark, $\bar{b}$ quark and the gluon) are combined into jets using the inclusive k_t jet-algorithm (in the E_t-scheme). The b-quark is then fragmented to a B-Hadron using the Peterson fragmentation function [19] with a fragmentation parameter

$\epsilon = 0.0033$. The B-Hadron subsequently decays into a muon. The muon spectrum takes both direct and cascade decays via charm into account.

The calculation is performed for a b-quark mass of 4.75 GeV with factorisation and renormalisation scales defined as $\mu_R = \mu_F = \sqrt{Q^2 + 4m_b^2}$. For the structure functions the DIS-scheme parametrisations CTEQ5F3 [14] for the proton is used. Systematic errors are estimated by varying the b-quark mass up and down by 0.25 GeV and μ_R and μ_F up and down by factors of two. The systematic error is estimated by simultaneous variation of the b-quark mass, μ_R = μ_F up and down respectively by 0.25 GeV and a factor two. The cross section variation when using other proton structure functions such as GRV98 or CTEQ4F3 is less than 8% in all regions of the measurement. The uncertainty due to variations of the fragmentation parameter ϵ by 25% is below 3%. This leads to a total uncertainty of +13% -20%.

The obtained parton level cross sections are corrected to the hadron level using the RAPGAP Monte Carlo generator. The corrections are on the level of 20% in all bins of the measurement decreasing towards larger $p_{t,jet}$. The shape comparison of the RAPGAP Monte Carlo with HVQDIS calculation gives a good description of the muon and the jet variables.

5 Determination of Signal and Background Components

The two observables δ and p_T^{rel} are used to determine the fraction of the beauty component in the data. Decays of long-lived particles are signalled by positive impact parameters, whereas the finite track resolution yields a symmetric distribution centered on zero. The transverse momentum p_T^{rel} of the muon track is calculated relative to the momentum of the associated jet after subtraction of the muon momentum. The details of the signal and background determination have been described in [7].

The two observables δ and p_T^{rel} are complementary in the discrimination of the beauty component in the data from the background sources and the fraction of beauty events in the data is determined from a combined fit to the two-dimensional distribution of δ and p_T^{rel}. The fit uses the shapes of the distributions of beauty, charm and light quark events from the RAPGAP Monte Carlo simulation. The relative weights of all three components are adjusted such that the likelihood is maximized. The overall normalisation of the summed contributions is adjusted to match the data. The fit yields a sample composition of $f_b = (31.1 \pm 3.7)\,\%$ (beauty), $f_c = (49.9 \pm 7.2)\,\%$ (charm) and $f_{uds} = (19.0 \pm 7.0)\,\%$ (uds). Here the errors refer to the statistical uncertainties.

The quality of the description of the data sample using the fractions obtained with the two-dimensional fit is demonstrated using the one-dimensional δ and p_T^{rel} projections. Figure 1 shows the measured impact parameter distribution in the data together with histograms indicating the contributions from b-production and from the c and uds backgrounds using the relative fractions obtained in the two-dimensional fit. The data are well described by the sum of the estimated contributions. In figure 2 the observed p_t^{rel} distribution is shown. The histogram represents the summed contributions from b-production and from the backgrounds, using the fractions determined above. As for the impact parameter, also the distribution of p_T^{rel} is well described by the sum of the estimated contributions.

The b-fraction can be enriched significantly by cuts in the distributions of p_T^{rel} and/or δ . Figures 3 and 4 show the result for regions of high b-purity, i.e. $p_T^{rel} > 1.2$ GeV and $\delta > 0.01$ cm, respectively. Also these high b-purity data are reasonably well described with the estimated contributions, derived from the results of the above two-dimensional fit.

Figure 5 shows the kinematic distributions of the selected events as obtained from data together with the expectations of the RAPGAP Monte Carlo simulation using the fractions of beauty, charm and light quarks obtained from the two-dimensional fit. Figure 6 shows the distributions of the muon transverse momentum p_T^{μ}, the pseudorapidity η^{μ}, the transverse momentum p_t^{*jet} of the highest-p_t jet in the Breit frame and of the same jets in the lab-frame and the jet-multiplicity distributions.

The data are adequately described by the simulation. The total systematic error is estimated to be 17% with contributions of similar size ($\sim 7\%$) due to track resolution uncertainties, muon identification uncertainty and dependence on the physics model. The latter is studied by using for the modeling of beauty and charm events alternatively the CASCADE Monte Carlo simulation and by using either Peterson [19] or Lund [20] fragmentation.

6 Results

The cross section measurements reported here are obtained from the likelihood fit to the two-dimensional distribution of p_T^{rel} and δ. The number of beauty events in the data, as estimated from the fit, is translated into a cross section by dividing by the detector acceptance, the efficiency and the integrated luminosity. The detector acceptances and efficiencies are determined from the RAPGAP Monte Carlo simulation.

The jet-muon beauty production cross section, $\sigma_{vis}(ep \to eb\bar{b}X \to ej\mu X)$, is measured in the visible range $2 < Q^2 < 100$ GeV^2, $0.1 < y < 0.7$, $p_T^{\mu} > 2.5$ GeV, $-0.75 < \eta^{\mu} < 1.15$, $p_t^{*jet} > 6$ GeV and $|\eta^{jet}| < 2.5$. The muon must be associated with the jet. The cross section is defined for jets which include all final state particles. The visible cross section is measured as

$$\sigma_{vis}(ep \to eb\bar{b} \to ej\mu X) = (8.8 \pm 1.0(stat.) \pm 1.5(sys.))\text{pb}.$$

In comparison the prediction from the NLO QCD calculation including corrections for fragmentation and hadronisation is $(7.3^{+1.0}_{-1.5})$ pb.

The differential cross sections are measured as function of the negative transverse momentum squared of the exchanged photon Q^2 (figures 7 and 8), the scaling variable x (figures 9 and 10) and the transverse momentum of the muon jet in the Breit frame, $p^*_{t,jet}$ (figures 11 and 12). The cross section values are determined separately for each bin, using the beauty fraction from the fit to the two-dimensional distribution of p_T^{rel} and δ in that bin. The cross section is obtained by dividing the number of beauty events from the fit by the detector acceptance and efficiency, the integrated luminosity and the width of the bin.

The data are compared with expectations obtained from the RAPGAP and CASCADE generators and the prediction from the QCD NLO calculation. All generators, RAPGAP and CASCADE, give a good description of the shapes of the distributions observed in the data. The RAPGAP prediction is too low in normalization. The NLO calculations show good agreement with the data.

7 Conclusions

A new measurement of beauty production cross sections performed with the H1 detector at HERA is presented. The analysis uses semi-muonic decays of b-flavoured hadrons and exploits their lifetime and mass properties in a simultaneous fit to the impact parameter and relative transverse momentum distribution of the decay muons. The total visible jet-muon cross section, defined in the region $2 < Q^2 < 100$ GeV^2, $0.1 < y < 0.7$, $p_T^{\mu} > 2.5$ GeV, $-0.75 < \eta^{\mu} < 1.15$, $p_t^{*jet} > 6$ GeV and $|\eta^{jet}| < 2.5$, is measured to be $(8.8 \pm 1.0(stat.) \pm 1.5(sys.))$ pb.

The cross sections are also measured differentially in Q^2, x and $p^*_{t,jet}$. Monte Carlo generators show reasonable agreement with the shapes of the data. RAPGAP is lower than the data by about a factor of two. The NLO calculations show good agreement with the data. The prediction for the total visible jet-muon cross from the NLO QCD calculation including fragmentation and hadronisation corrections as described in section 4 is $(7.3^{+1.0}_{-1.5})\mathrm{pb}$.

References

[1] C. Adloff *et al.* [H1 Collaboration], Phys. Lett. B **467** (1999) 156 [Erratum-ibid. B **518** (2001) 331] [hep-ex/9909029].

[2] H1 Collaboration, Cont. paper to the ICHEP 2000 conference, Osaka, Japan, July 2000.

[3] J. Breitweg *et al.* [ZEUS Collaboration], Eur. Phys. J. C **18** (2001) 625 [hep-ex/0011081].

[4] CDF Coll., F. Abe *et al.*, Phys. Rev. Let. 71 (1993) 2396, Phys. Rev. D 53 (1996) 1051; D0 Coll., S. Abachi *et al.*, Phys. Rev. Let 74 (1995) 3548, Phys. Let. B 370 (1996) 239.

[5] M. Acciarri *et al.* [L3 Collaboration], Phys. Lett. B **503**, 10 (2001) arXiv:hep-ex/0011070.

[6] S. Chekanov *et al.* [ZEUS Collaboration], arXiv:hep-ex/0312057.

[7] A.Aktas *et al.* [H1 Collaboration], paper contributed to the International Europhysics Conference, 2003, Aachen.

[8] I. Abt *et al.* [H1 Collaboration], Nucl. Instrum. Meth. A **386** (1997) 310 and 348.

[9] D. Pitzl *et al.*, Nucl. Instrum. Meth. A **454**, 334 (2000) arXiv:hep-ex/0002044.

[10] T. Nicholls *et al.* [H1 SPACAL Group Collaboration], Nucl. Instrum. Meth. A **374** (1996) 149.

[11] U. Bassler, G. Bernardi, Nucl.Instrum.Meth.A361:197-208,1995 hep-ex/9412004

[12] S. Catani, Yu. Dokshitzer, M.H.Seymour and B.R. Webber, Nucl. Phys. B 406 (1993) 187.

[13] H. Jung, Comput. Phys. Commun. **86** (1995) 147.

[14] L. Lai *et al.* [hep-ph/9903282].

[15] T. Sjostrand, Comput. Phys. Commun. **82** (1994) 74.

[16] H. Jung and G. P. Salam, Eur. Phys. J. C **19** (2001) 351 [hep-ph/0012143];
H. Jung, Comput. Phys. Commun. **143** (2002) 100 [hep-ph/0109102].

[17] M. Ciafaloni, Nucl. Phys. B **296** (1988) 49;
S. Catani, F. Fiorani and G. Marchesini,
Phys. Lett. B **234** (1990) 339, Nucl. Phys. B **336** (1990) 18;
G. Marchesini, Nucl. Phys. B **445** (1995) 49.

[18] B.W. Harris and J. Smith, NUCL. PHYS. B **452** (1995) 109.

[19] C. Peterson, D. Schlatter, I. Schmitt, and P.M. Zerwas, Phys. Rev. D 27 (1983) 105.

[20] T. Sjöstrand, Comput. Phys. Commun. **82** (1994) 74.

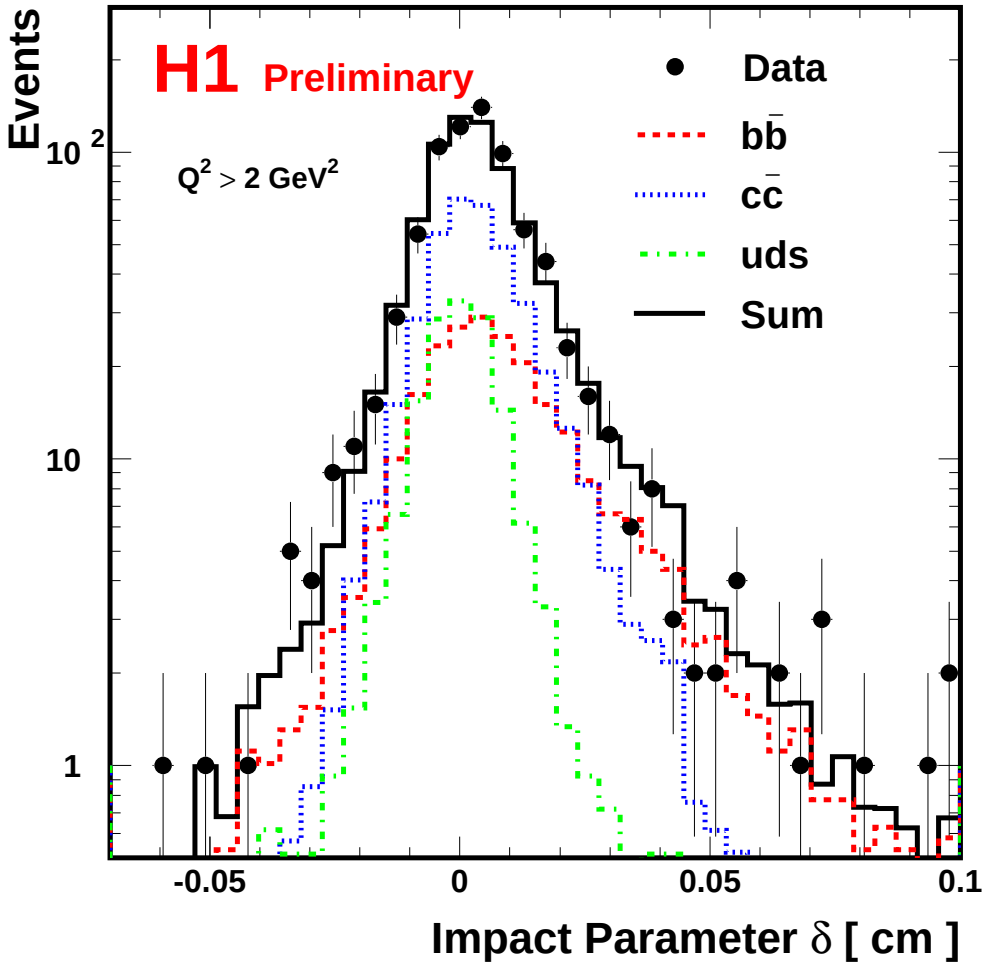

Figure 1: Distribution of the impact parameter δ of the muon track. The data (points) are compared with the RAPGAP Monte Carlo simulation (solid line). The decomposition into the b (dashed line), the c (dotted line) and the light quark (dash-dotted line) components is determined from a fit to the two-dimensional distribution of p_T^{rel} and δ (see text).

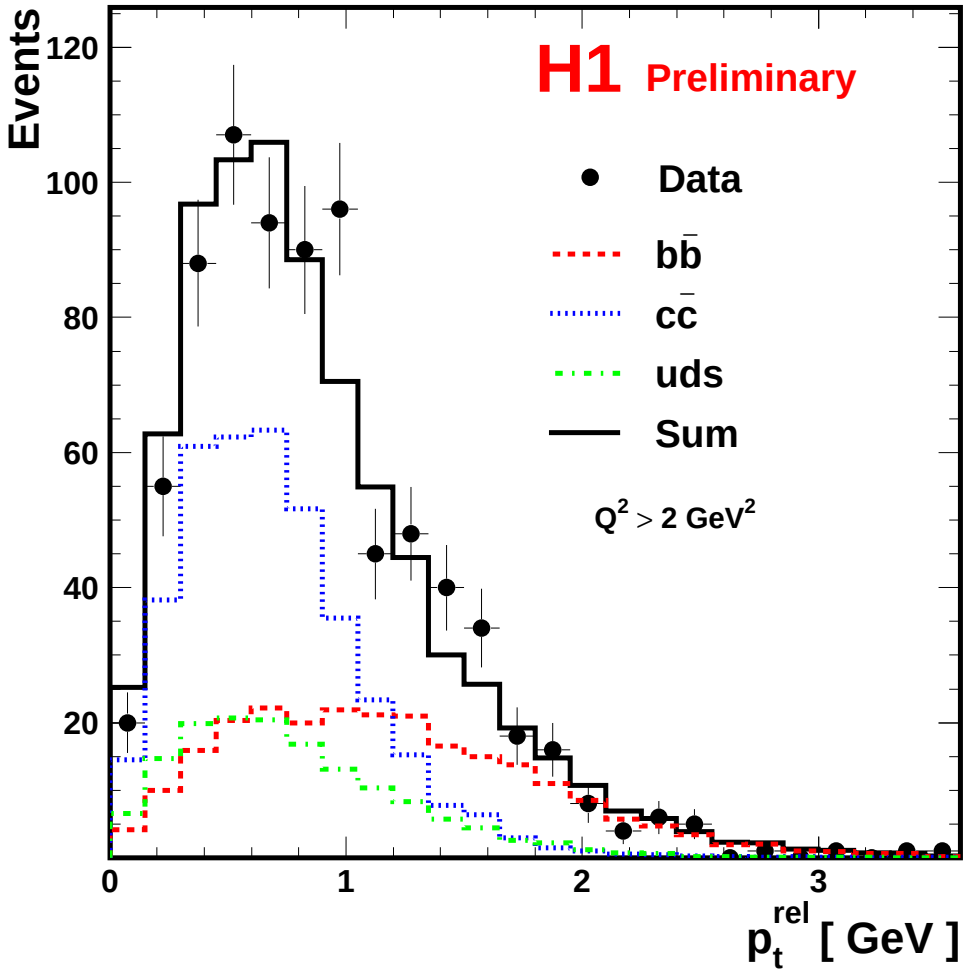

Figure 2: Distribution of transverse muon momentum p_T^{rel} relative to the jet axis. The data (points) are compared with the RAPGAP Monte Carlo simulation (solid line). The decomposition into the b (dashed line), the c (dotted line) and the light quark (dash-dotted line) components is determined from a fit to the two-dimensional distribution of p_T^{rel} and δ (see text).

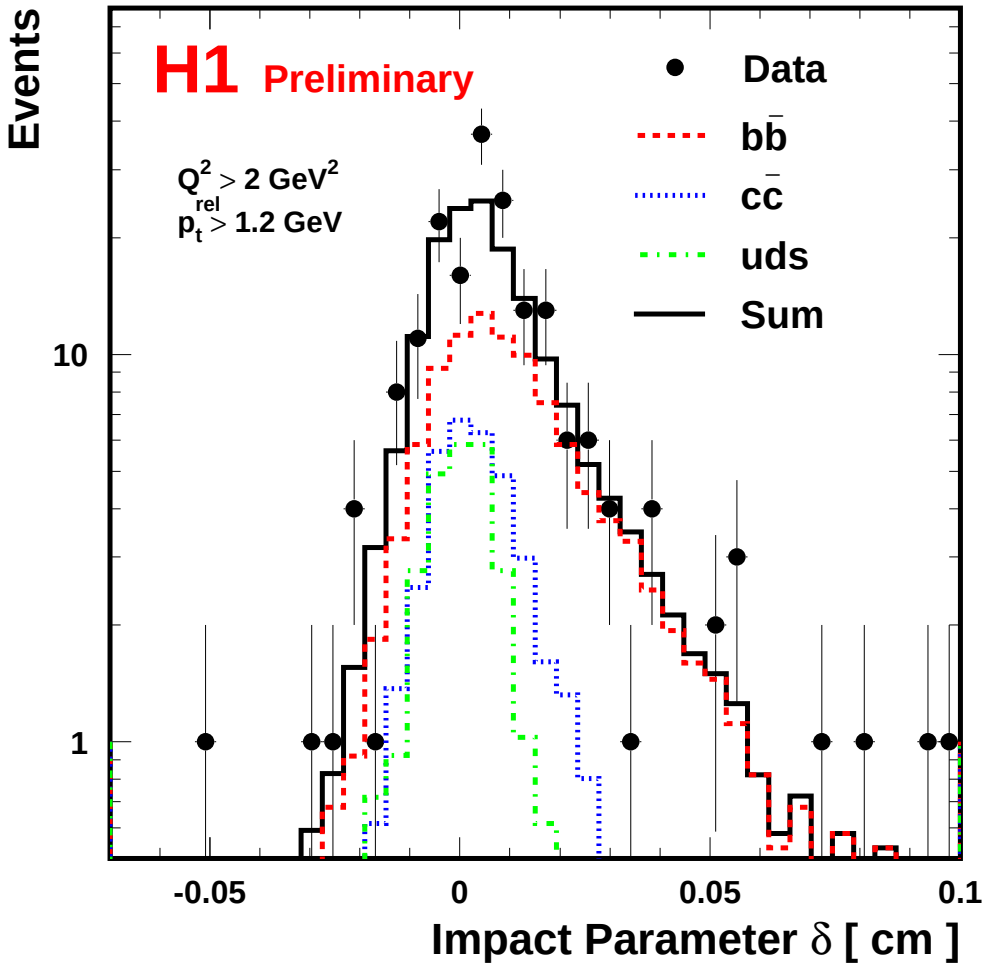

Figure 3: Distribution of the impact parameter δ of muon tracks with enhanced b-fraction by a cut on $p_T^{rel} > 1.2$ GeV The data (points) are compared with the RAPGAP Monte Carlo simulation (solid line). The b, c and uds fractions are fixed from the same combined fit to δ and p_T^{rel} as for figures 2 and 1.

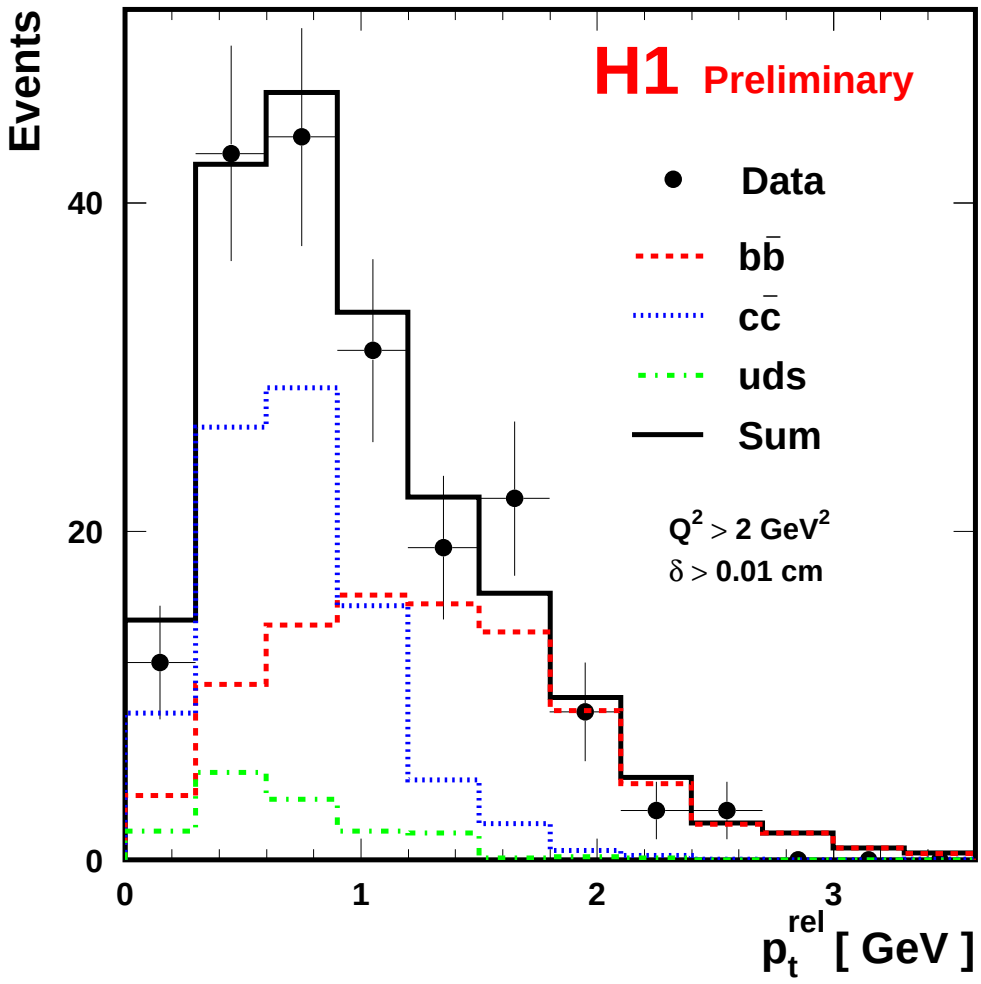

Figure 4: Distribution of transverse muon momentum p_T^{rel} relative to the jet axis for events with an impact parameter $\delta > 0.01$ cm. The data (points) are compared with the RAPGAP Monte Carlo simulation (solid line). The b, c and uds fractions are fixed from the same combined fit to δ and p_T^{rel} as for figures 2 and 1.

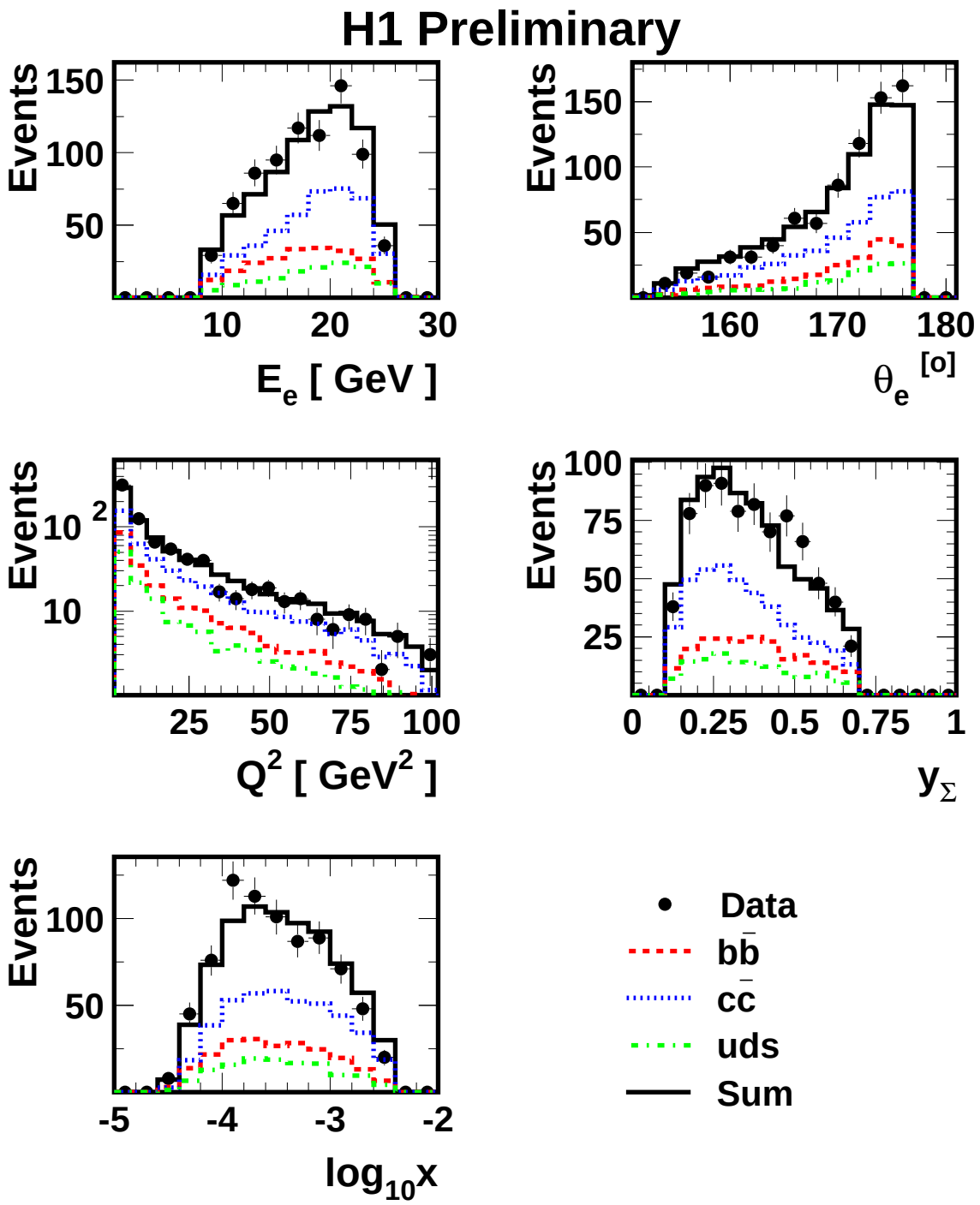

Figure 5: Distribution of the scattered electron energy and polar angle, the photon virtuality Q^2 and inelasticity y as well as logarithm of the scaling variable x. The data are compared to the RAPGAP Monte Carlo simulation. The estimated contributions of beauty, charm and light quark events, taken from the fit result, are shown as separate curves.

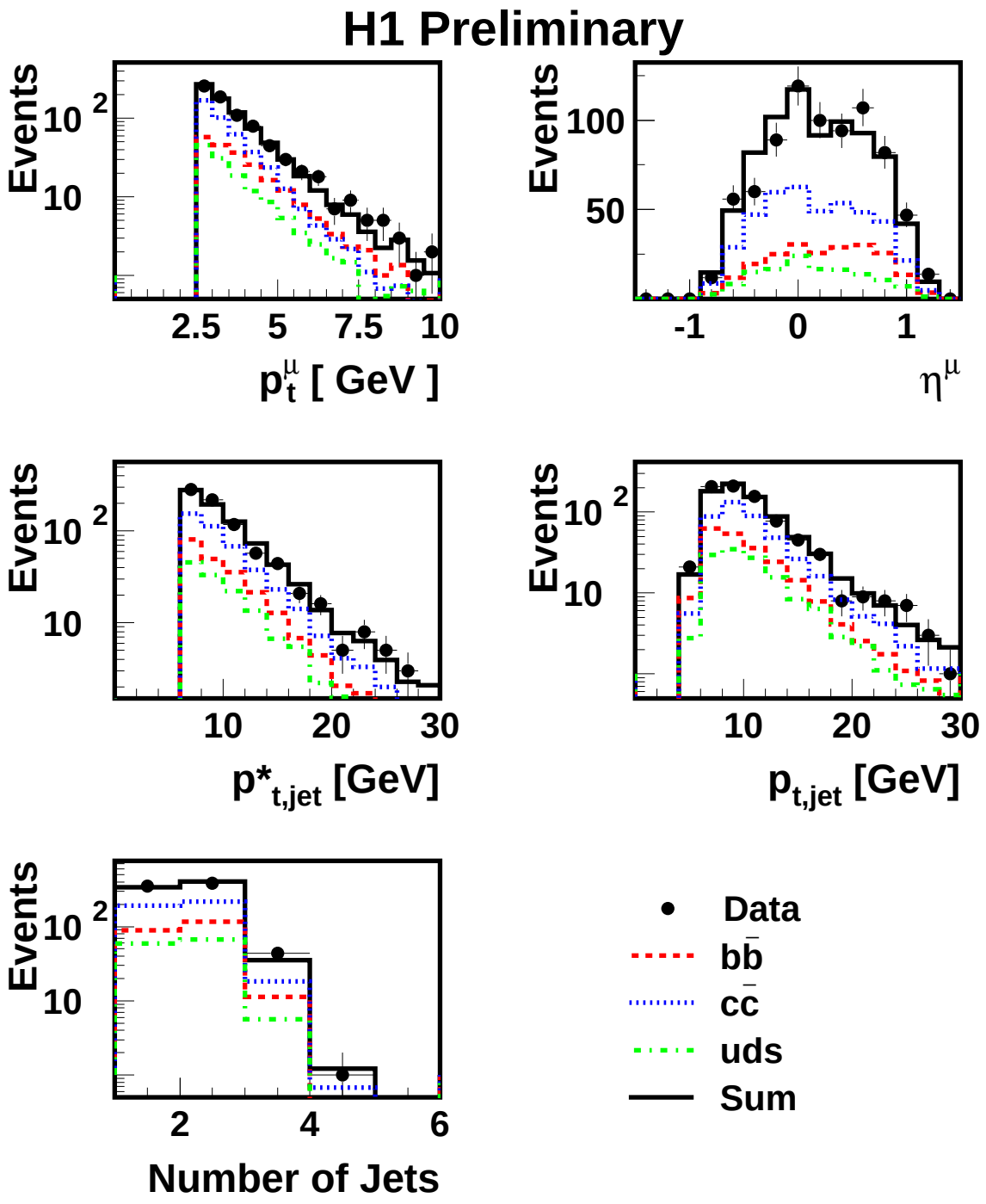

Figure 6: Distributions of the muon transverse momentum p_T^μ, the pseudorapidity η^μ, the transverse momentum of the jet in the laboratory frame p_t^{jet} and in the Breit frame p_t^{*jet} and the jet multiplicity. The data are compared to the RAPGAP Monte Carlo simulation. The estimated contributions of beauty, charm and light quark events, taken from the fit result, are shown as separate curves.

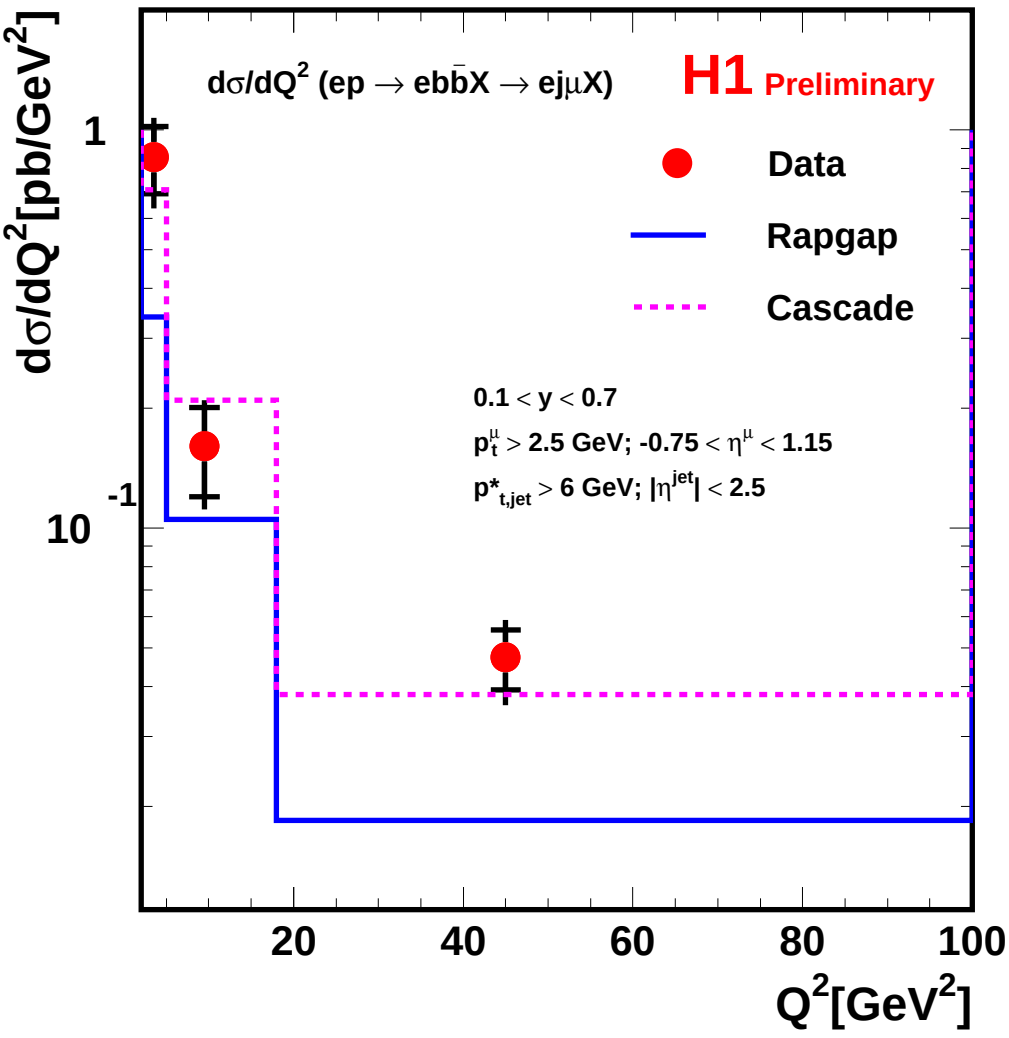

Figure 7: Differential dijet muon beauty production cross section $d\sigma/dQ^2(ep \rightarrow eb\bar{b}X \rightarrow ej\mu X)$ as a function of Q^2 in the range $100 > Q^2 > 2$ GeV^2, $0.1 < y < 0.7$, $p_T^{\mu} > 2.5$ GeV, $-0.75 < \eta^{\mu} < 1.15$, $p_t^{*jet} > 6$ GeV and $|\eta^{jet}| < 2.5$. The inner error bars show the statistical error, the outer error bars represent the statistical and systematic uncertainty added in quadrature. Also shown are the predictions from the Monte Carlo generator programs RAPGAP (solid line) and CASCADE (dashed line).

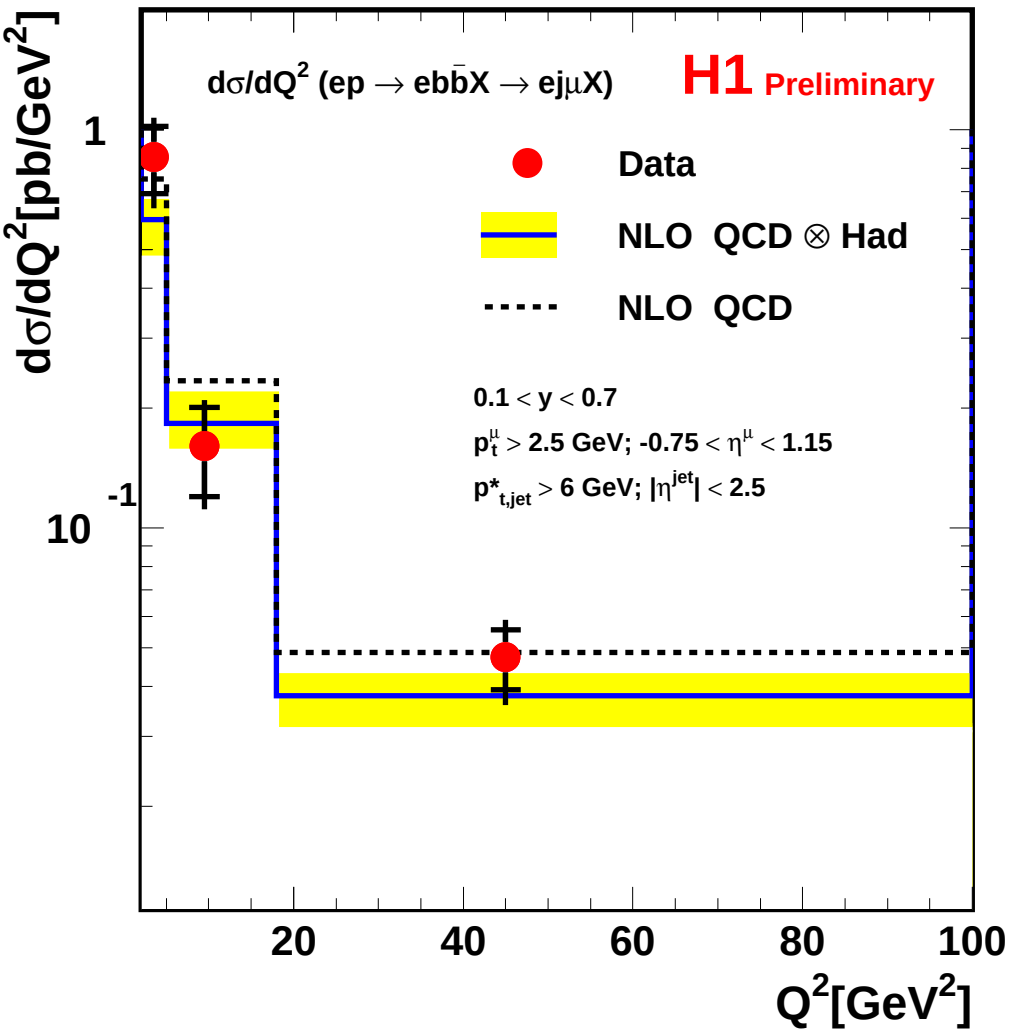

Figure 8: Differential dijet muon beauty production cross section $d\sigma/dQ^2(ep \rightarrow eb\bar{b}X \rightarrow ej\mu X)$ as a function of Q^2 in the range $100 > Q^2 > 2$ GeV^2, $0.1 < y < 0.7$, $p_T^{\mu} > 2.5$ GeV, $-0.75 < \eta^{\mu} < 1.15$, $p_t^{*jet} > 6$ GeV and $|\eta^{jet}| < 2.5$. The inner error bars show the statistical error, the outer error bars represent the statistical and systematic uncertainty added in quadrature. Also shown is the prediction from a pQCD NLO calculation [18] at parton level (dashed line) and hadron level (solid line). The band shows the uncertainty obtained from variations of the b-quark mass, μ_r and μ_f (see text).

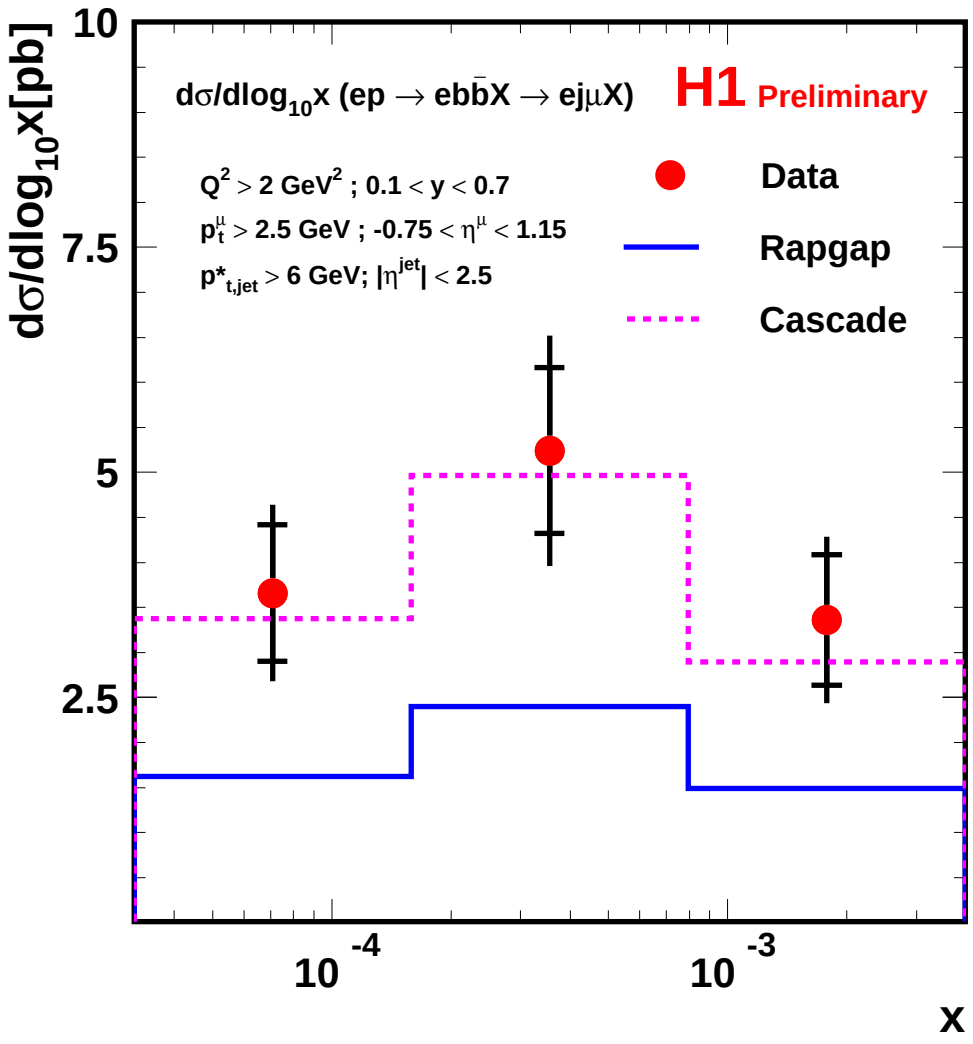

Figure 9: Differential dijet muon beauty production cross section $d\sigma/d\log x(ep \to eb\bar{b}X \to ej\mu X)$ as a function of x in the range $100 > Q^2 > 2$ GeV^2, $0.1 < y < 0.7$, $p_T^{\mu} > 2.5$ GeV, $-0.75 < \eta^{\mu} < 1.15$, $p_t^{*jet} > 6$ GeV and $|\eta^{jet}| < 2.5$. The inner error bars show the statistical error, the outer error bars comprise the statistical and systematic uncertainty added in quadrature. Also shown are the predictions from the Monte Carlo generator programs RAPGAP (solid line) and CASCADE (dashed line).

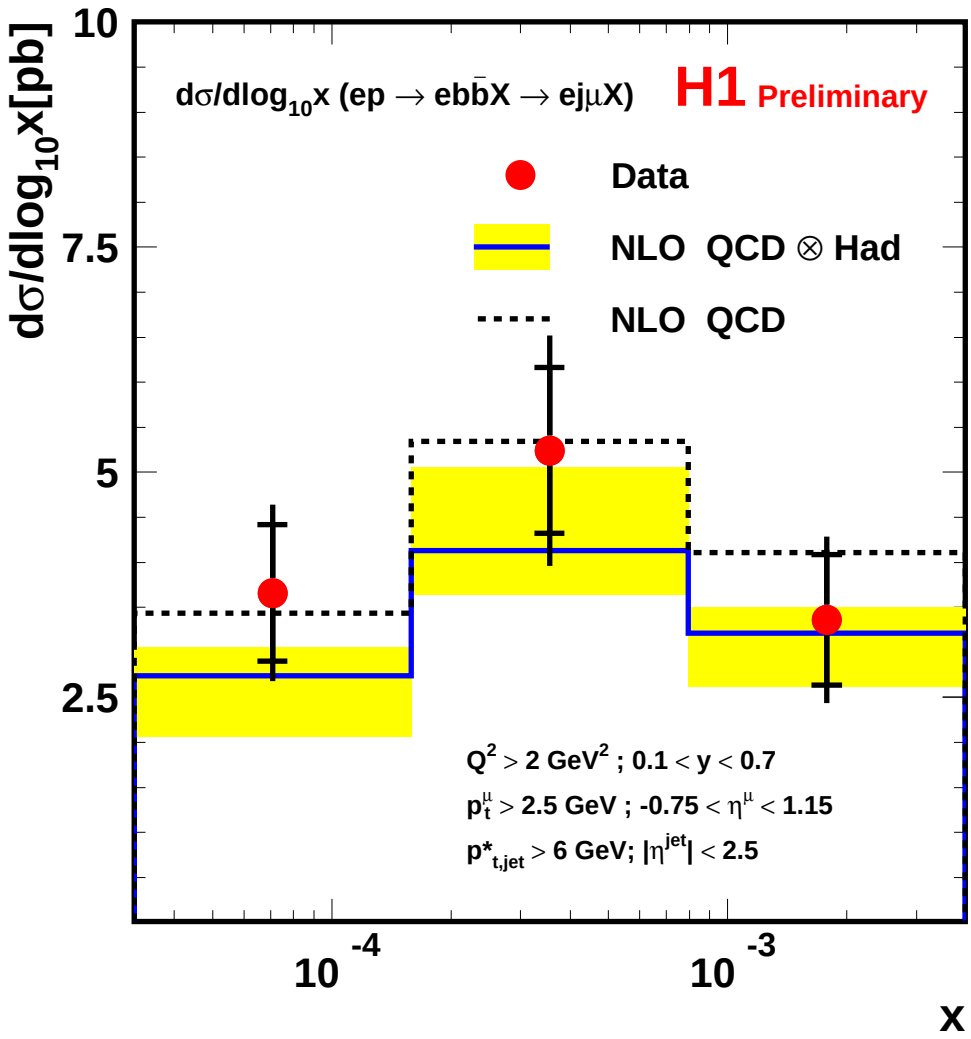

Figure 10: Differential dijet muon beauty production cross section $d\sigma/d\log x(ep \to eb\bar{b}X \to ej\mu X)$ as a function of x in the range $100 > Q^2 > 2$ GeV^2, $0.1 < y < 0.7$, $p_T^{\mu} > 2.5$ GeV, $-0.75 < \eta^{\mu} < 1.15$, $p_t^{*jet} > 6$ GeV and $|\eta^{jet}| < 2.5$. The inner error bars show the statistical error, the outer error bars comprise the statistical and systematic uncertainty added in quadrature. Also shown is the prediction from a pQCD NLO calculation [18] at parton level (dashed line) and hadron level (solid line). The band shows the uncertainty obtained from variations of the b-quark mass, μ_r and μ_f (see text).

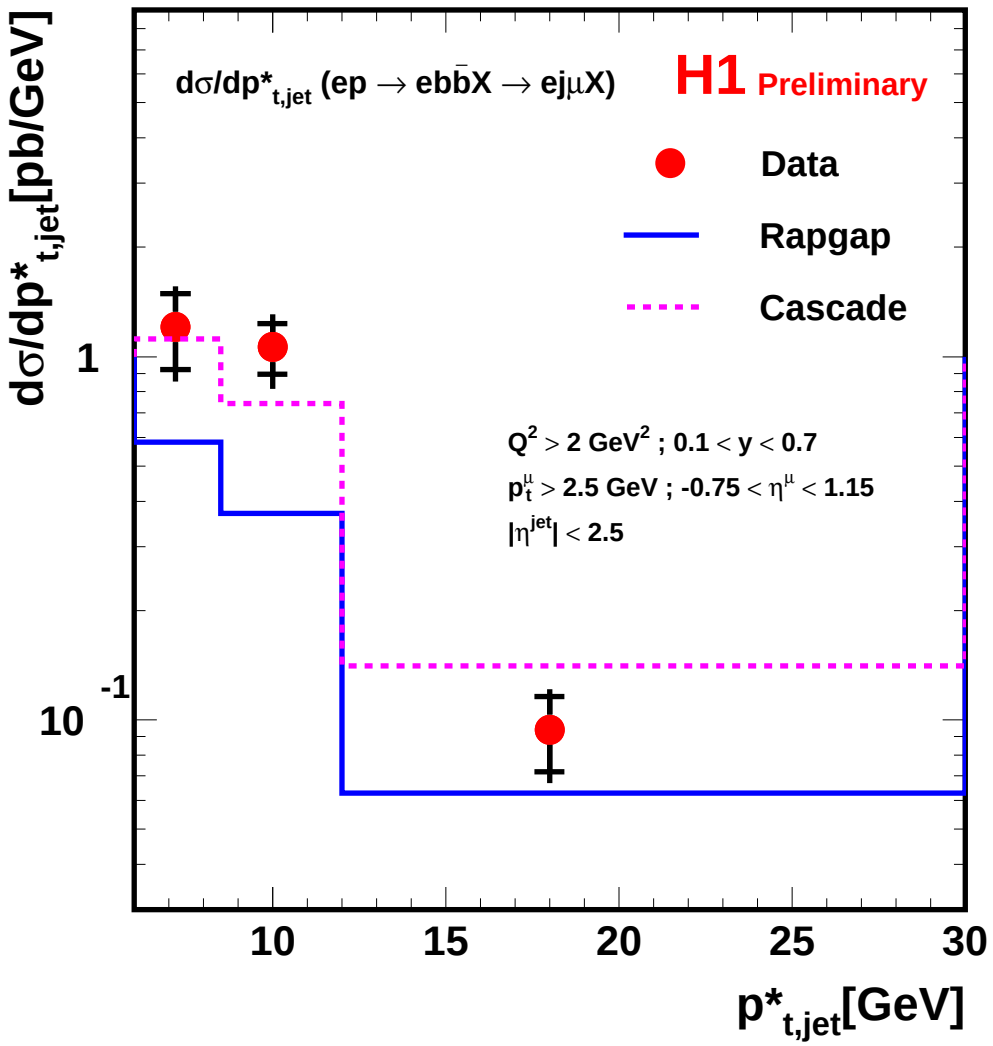

Figure 11: Differential dijet muon beauty production cross section $d\sigma/dp^*_{t,jet}(ep \to eb\bar{b}X \to ej\mu X)$ as a function of $p^*_{t,jet}$ in the Breit frame, in the range $100 > Q^2 > 2$ GeV^2, $0.1 < y < 0.7$, $p^\mu_T > 2.5$ GeV, $-0.75 < \eta^\mu < 1.15$ and $|\eta^{jet}| < 2.5$. The inner error bars show the statistical error, the outer error bars comprise the statistical and systematic uncertainty added in quadrature. Also shown are the predictions from the Monte Carlo generator programs RAPGAP (solid line) and CASCADE (dashed line).

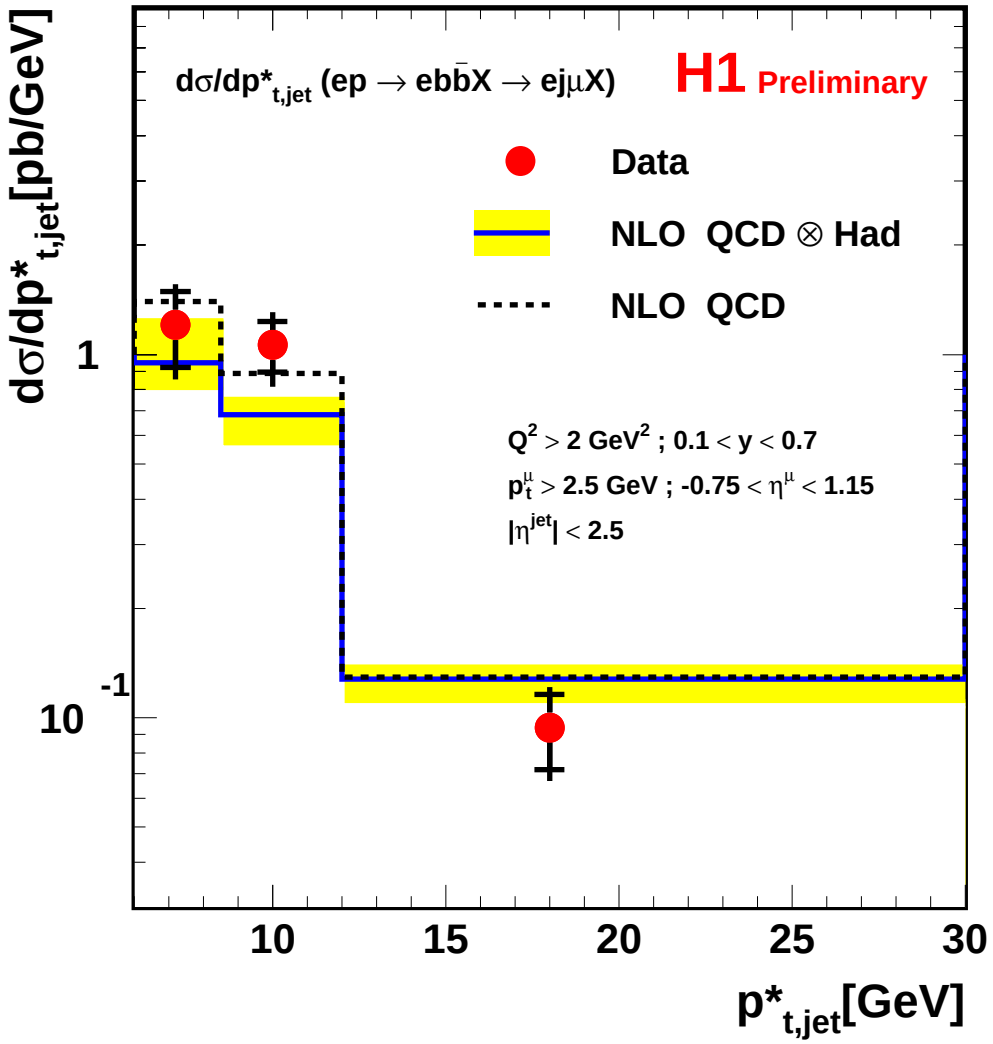

Figure 12: Differential dijet muon beauty production cross section $d\sigma/dp^*_{t,jet}(ep \to eb\bar{b}X \to ej\mu X)$ as a function of $p^*_{t,jet}$ in the Breit frame, in the range $100 > Q^2 > 2$ GeV^2, $0.1 < y < 0.7$, $p^\mu_T > 2.5$ GeV, $-0.75 < \eta^\mu < 1.15$ and $|\eta^{jet}| < 2.5$. The inner error bars show the statistical error, the outer error bars comprise the statistical and systematic uncertainty added in quadrature. Also shown is the prediction from a pQCD NLO calculation [18] at parton level (dashed line) and hadron level (solid line). The band shows the uncertainty obtained from variations of the b-quark mass, μ_r and μ_f (see text).